Journal of Thermal Analysis, Vol. 50 (1997) 745-756

THERMAL DECOMPOSITION OF Cu-BASED HYDROXYCARBONATE CATALYTIC PRECURSORS FOR THE LOW-TEMPERATURE CO-SHIFT REACTION

*M. J. L. Ginés and C. R. Apesteguía**

Instituto de Investigaciones en Catálisis y Petroquímica (INCAPE), UNL-CONICET
Santiago del Estero 2654, (3000) Santa Fe, Argentina

(Received April 26, 1996; in revised form November 10, 1996)

Abstract

The thermal decomposition of Cu–Zn–Al hydroxycarbonate precursors to obtain water-gas shift catalysts was studied by employing a variety of experimental techniques. A set of six samples containing 34 wt% of Cu and different Al/Zn ratios were prepared by coprecipitation. Depending on the cation ratio, the ternary precursors contained hydrotalcite, aurichalcite and/or rosasite phases. Malachite and hydrozincite were determined in binary Cu/Al and Cu/Zn samples, respectively. The precipitates decomposed in three endothermic transformations in the temperature ranges 363–453 K, 453–673 K and 673–923 K. In the first step (ΔW=0–9%), the hydrotalcite-containing samples lost the crystallization water of the hydrotalcite phase. In the middle-temperature transition (ΔW=18–30%), the samples were completely dehydroxylated and simultaneously eliminated a proportion of the carbonate ions through a two-step dehydroxylation/decarbonation process. The high-temperature transformation (ΔW=3–7%) corresponded to the final decarbonation of the samples. Mixed oxides with a high dispersion of copper were obtained from hydrotalcite-containing precursors: the higher the amount of hydrotalcite in the precursor, the lower the CuO crystallite size in the resulting mixed oxide.

Keywords: CO-shift reaction, Cu-based hydrocarbonates, thermal decomposition

Introduction

From many years, $Cu/ZnO/Al_2O_3$ catalysts have been employed for the low-temperature CO-shift reaction ($CO+H_2O \rightleftarrows CO_2+H_2$), which is applied industrially to produce hydrogen or ammonia from synthesis gas. The exact nature of the active sites in these Cu–Zn–Al catalysts is still debated, but there is general agreement that Cu is the active metal for this reaction [1, 2]. More active cata-

* Author to whom all correspondence should be addressed.

0368–4466/97/ $ 5.00
© 1997 Akadémiai Kiadó, Budapest
John Wiley & Sons Limited
Chichester

lysts are effectively obtained when Cu is highly dispersed on ZnO/Al_2O_3 matrix [3]. On the other hand, in commercial practice the reactor temperature is raised to compensate catalyst deactivation caused by the presence of poisons, particularly chlorine. Because of thermal sintering, the lifetime of the catalyst may be shortened through the constant elevation of the operating temperature. To limit catalyst deactivation by Cu sintering, the metal should be homogeneously distributed in small metallic crystallites across the support. Thus, the preparation of mixed oxides with a high Cu dispersion appears to be an essential factor for improving both the activity and the resistance to thermal sintering of Cu–Zn–Al catalysts.

In general, the physicochemical properties of the resulting mixed oxides depend on the precursor homogeneity and on the characteristics of the decomposition and calcination steps [4, 5]. Hadden *et al.* [6] studied the impact of precipitation and ageing parameters on the activity of $Cu/ZnO/Al_2O_3$ shift catalysts and found that discrete Cu area-activity relationships were evident within groups of catalysts obtained under identical preparation conditions. Baker *et al.* [7] noted that in Cu-based catalysts the thermal activation has a pronounced effect on the catalytic performance. In agreement with this, we recently established [8] that the activity of CO-shift catalysts continuously decreases when the calcination temperature is increased, starting from 673 K, but a drastic drop in activity is observed only upon calcination of the sample at temperatures higher than 873 K. A better understanding of the relationship between active site formation and the chemistry of the catalyst preparation is needed. In this paper we have studied the thermal decomposition of different Cu–Zn–Al coprecipitated precursors in order to specifically determine the influence the precursor phase composition has on the CuO crystallite size of the resulting mixed oxides.

Experimental

Catalytic precursors were prepared by coprecipitation from an aqueous solution of the metal nitrates with sodium carbonate at 333 K and $pH=7.2\pm0.2$ in a stirred batch reactor, according to Ref. [4]. The precipitates were filtered off, washed with distilled water at 333 K until the disappearance of Na^+, and dried at 363–373 K overnight. A set of samples containing two (Cu–Al or Cu–Zn) or three (Cu–Zn–Al) metal components was prepared. After the thermal decomposition, all the samples contained 34% of Cu, as determined by atomic absorption spectrometry. The nomenclature and chemical compositions of the samples are shown in Table 1.

The thermal decompositions of the precursors were studied by means of differential thermal analysis (DTA), thermogravimetry (TG), and derivative thermogravimetry (DTG), using a Shimadzu DT-30 thermal analyzer and a Cahn 2000 electrobalance. In DTA experiments, the temperature was raised at 10 K min^{-1} from 298 to 873 K. Samples weighing 10 mg were heated in quartz dishes under a flow of nitrogen (50 cm^3 min^{-1}). TG studies were carried out at

1 atm in a flow system. Powder samples (15–20 mg) were placed on a glass container suspended vertically and heated under nitrogen with a flow rate of 20 cm^3 min^{-1}. The temperature was raised with a linear temperature programmer-controlled electric furnace at 5 K min^{-1} within the temperature range 298–973 K.

The precursor decomposition was also characterized by temperature-programmed decomposition and evolved gas analysis (EGA). The experiments were carried out at atmospheric pressure in a flow system provided with a fixed-bed reactor. Approximately 350 mg was heated in He at 5 K min^{-1} from room temperature up to 873 K. Gases were sampled from a quartz reactor positioned in a temperature-programmed furnace. The gaseous effluent was analyzed by gas chromatography, using a thermal conductivity detector and a Porapak QS column.

X-ray diffraction (XRD) patterns were collected in a Rich-Seifert diffractometer, using nickel-filtered CuK_α radiation. The CuO crystallite sizes (L_{CuO}) were evaluated from the CuO (111) diffraction lines, using the Sherrer equation. Infrared spectra were recorded with Shimadzu 8100 equipment provided with a diffuse reflectance cell and a DRIFT MCT detector. Spectra were measured at room temperature between 1800 and 400 cm^{-1}. Thin sample wafers were formed by pressing approximately 50 mg of the precursor powder at a pressure of around 5 ton cm^{-2}. BET surface areas (S_g) were measured by N_2 adsorption at 77 K in a Micromeritics Accusorb 2100 sorptometer.

Results and discussion

Precursor characterization

XRD techniques were used for qualitative determination of the compositions of all the precursors. Results are shown in Table 1. Depending on the chemical composition, different hydroxycarbonate phases were detected: hydrotalcite [$(Cu,Zn)_6Al_2CO_3(OH)_{16}\cdot 4H_2O$], rosasite [$(Cu,Zn)_2CO_3(OH)_2$], aurichalcite [$(Cu,Zn)_5(CO_3)_2(OH)_6$], hydrozincite [$Zn_5(CO_3)_2(OH)_6$], and malachite [$Cu_2CO_3(OH)_2$]. No traces of hydroxynitrate phases such as gherardite [$(Cu_2NO_3(OH)_3$] were detected. Hydrotalcite was selectively obtained as a single phase only in sample T-2, which has a (Cu+Zn)/Al atomic ratio of 3, the stoichiometric M^{2+}/M^{3+} cation ratio of the hydrotalcite formulation. The ternary precursors T-1, T-3 and T-4 were heterogeneous: the hydrotalcite phase was accompanied by crystalline aurichalcite and/or rosasite phases. The result agrees with those from previous studies which demonstrated that hydrotalcite is selectively obtained by the coprecipitation method only for a rigid composition stoichiometry [4, 9]. On the other hand, hydrozincite was detected exclusively in binary sample B-2, whereas malachite was observed only in quasi-amorphous sample B-1.

Table 1 Composition and characterization of the catalytic precursors

Sample	(Cu+Zn)/Al[a]	Al/Zn[a]	Phases detected by XRD	S_g/m^2g^{-1}
B-1	0.6	∞	malachite (quasi-amorphous)	110
T-1	1.2	2.5	hydrotalcite	60
			rosasite (traces)	
T-2	3	0.65	hydrotalcite	43
T-3	4	0.50	hydrotalcite	39
			rosasite	
			aurichalcite (traces)	
T-4	6	0.30	aurichalcite	29
			rosasite (traces)	
B-2	∞	0	aurichalcite	23
			hydrozincite (traces)	

[a]atomic ratios

BET surface areas of the samples are also given in Table 1. The S_g values increased with the Al content, from 23 $m^2 g^{-1}$ (sample B-2, Al/Zn=0) to 110 $m^2 g^{-1}$ (sample B-1, Al/Zn=∞).

Precursor decomposition

TG-DTG and DTA results

The precipitates were subjected to combined TG and DTA analysis. The DTG and DTA curves are shown in Figs 1 and 2, respectively. Quantitative results of the mass losses detected during precursor decomposition are given in Table 2. The general patterns of the DTG and DTA curves allowed us to distinguish between three main endothermic phase transformations, in the temperature ranges 363–453 K, 453–673 K and 673–923 K. In the first step, the hydrotalcite-containing precursors (samples T-1, T-2 and T-3) exhibited an endothermic low-temperature peak at ca. 420–430 K. The mass losses (ΔW=3–9%) followed the order T-2>T-1>T-3 (Table 2). No decomposition peaks were detected for samples B-1, B-2 and T-4 in this low-temperature region.

The second transition of ternary samples was characterized by the presence of a broad, endothermic band between 453 and 673 K. The band maximum shifted to higher temperatures when the Al/Zn ratio was decreased, i.e. from sample T-1 to sample T-4. Binary sample B-2 exhibited a sharp endothermic peak at ca. 623 K, whereas the decomposition of sample B-1 in this middle-temperature range gave rise to two endothermic peaks, at about 493 K and 603 K. Sample mass losses varied between 18 and 30%.

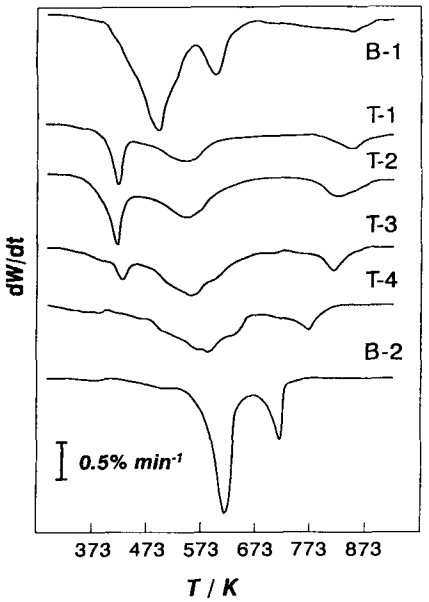

Fig. 1 DTA curves of the decompositions of precursors. Heating rate, 5 K min^{-1}. On the ordinate, W represents the percentage loss in mass

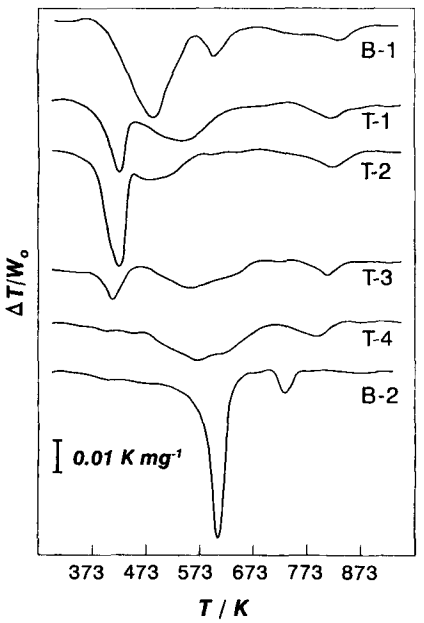

Fig. 2 DTA profiles of the decompositions of precursors. Heating rate, 10 K min^{-1}

Finally, all the samples presented a high-temperature endothermic transformation. Ternary samples and binary samples B-1 decomposed in a small, broad band in the region 673–923 K, whereas sample B-2 exhibited a sharp peak at 723 K. Above 673 K, the mass losses of the samples represented 3–7% of the initial mass.

Table 2 Decomposition of precursors: mass losses in the range 363–923 K

Sample	Mass loss/%[a]			Phase composition[b]	Total mass loss/%	
	363–453 K	453–673 K	673–923 K	%	Experimental	Predicted[c]
B-1	0	30.2	5.2	Ma(40)-Sc(60)	35.4	37.8
T-1	7.2	18.4	6.6	HT(84)-Ro(16)	31.2	30.3
T-2	8.5	18.8	3.4	HT(100)	30.7	30.8
T-3	3.1	19.9	4.7	HT(36)-Ro(64)	27.7	28.9
T-4	0.5	21.2	4.4	HT(5)-Au(95)	26.1	26.6
B-2	0	20.7	4.8	Au(100)	25.5	26.0

Ma=Malachite; Sc=Scarboite; HT=Hydrotalcite; Ro=Rosasite; Au=Aurichalcite
[a]Mass loss at consecutive temperature ranges (in % of the initial mass)
[b]Phase composition of the precursors postulated on the basis of XRD, DTG and EGA results
[c]Values calculated from the phase composition of the precursors (column 5)

The total mass loss for the six samples was between 25 and 35%. As revealed in Table 2, the mass loss increased as the Al/Zn ratio was increased.

EGA results

The general patterns of the EGA curves corresponded with the DTG and DTA profiles: thus, three main transitions were distinguished. Figure 3 shows the EGA results on ternary samples T-2 and T-3, while the EGA traces of binary samples B-2 and B-1 are presented in Fig. 4. In the range of the low-temperature tranformation, samples T-2 and T-3 eliminated water, whereas no evolved gas was detected for samples B-2 and B-1. The EGA curves of samples T-4 and T-1 (not shown here) confirmed that only the hydrotalcite-containing samples decomposed with the elimination of water in the range 363–453 K. The dehydration peak diminished in the order T-2>T-1>T-3, which is the sequence followed by the amount of hydrotalcite contained in the respective precursors, as established by XRD characterization. Structural investigations [10, 11] have shown that rhombohedral hydrotalcite-like compounds consist of positively charged brucite-like layers $[M_6^{2+}M_2^{3+}(OH)_{16}]^{2+}$ alternating with disordered negatively charged interlayers which contain the anions CO_3^{2-} and crystallization water. Our EGA results and results reported elsewhere [12, 13] lead us to attribute the low-temperature peak to crystallization water loss from the hydrotalcite phase.

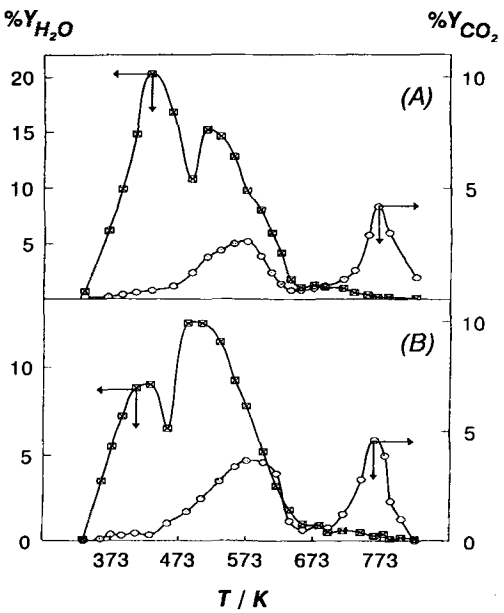

Fig. 3 EGA results on the decompositions of ternary precursors. Y_i% are the molar fractions of the gaseous products, including the helium carrier. (A) Sample T-2; (B) sample T-3

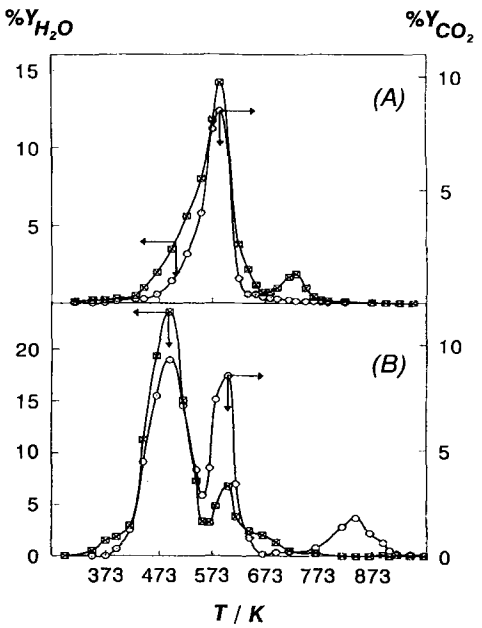

Fig. 4 EGA results on the decompositions of binary precursors. Y_i% are the molar fractions of the gaseous products, including the helium carrier. (A) Sample B-2; (B) sample B-1

As concerns the middle-temperature transition, Figs 3A and 3B show that the decompositions of samples T-2 and T-3 involved the successive elimination of H_2O and CO_2 in a two-step sequence; similar behavior was observed for sample T-1. The maximum in the H_2O curve was found at ca. 513 K. CO_2 was progressively removed at temperatures above 473 K, and, as a consequence, dehydroxylation overlapped with the onset of decarbonation. This partially overlapping elimination of water and CO_2 accounts for the broad bands observed in the corresponding DTG-DTA profiles of the ternary samples (Figs 1 and 2). In previous papers dealing with hydrotalcite decomposition, it was stated [14] that water is initially formed from adjacent OH groups in the same brucite-like layer and then from OH groups of contiguous layers, causing the lamellar structure to collapse. CO_2 arises from decomposition of the interlayer CO_3^{2-} [15]. As regards the binary samples, the EGA trace of sample B-2 (Fig. 4A) showed that water is eliminated together with CO_2 in the region 453–673 K, the respective peaks overlapping almost completely. This is consistent with the single decomposition peak observed at 623 K in the DTG/DTA profiles of sample B-2 (Figs 1 and 2). Since X-ray diffraction analysis demonstrated that sample B-2 was mostly aurichalcite (Table 1), we conclude that in the middle-temperature range aurichalcite decomposes in a one-step process by simultaneously eliminating the CO_3^{2-} and the OH groups. On the other hand, binary sample B-1 decomposed in a two-step transition at 493 and 603 K, releasing CO_2 together with water (Fig. 4B). X-ray characterization of precursor B-1 revealed the presence of malachite in a quasi-amorphous diffractogram (Table 1). Previous work demonstrated that malachite decomposes in a single peak at 590–623 K [16], and we attribute the 603 K decomposition peak for sample B-1 to decomposition of the malachite phase contained in the precipitate precursor. The first peak, at 493 K, is assigned to the decomposition of an amorphous hydroxycarbonate phase, probably a scarboite-like phase [$Al_2(CO_3)_3 \cdot 12\,Al(OH)_3$]. The formation of scarboite in precursors with compositions similar to that of sample B-1 has already been reported [17].

Finally, Figs 3 and 4 showed that only CO_2 was released above 673 K, thereby indicating that the high-temperature decomposition region between 673 and 923 K corresponded to the final decarbonation of samples T-2, T-3, B-1 and B-2. Similar results were obtained for samples T-1 and T-4. The CO_2 peak shifted slightly to higher temperatures as the Al content on the samples was increased.

The XRD/DTG/EGA results allowed us to postulate the possible phase compositions of precipitate precursors. In ternary samples, the amount of hydrotalcite was calculated by considering that the low-temperature mass loss arose only from the crystallization water loss of the hydrotalcite phase. The phase composition of sample B-1 was estimated by assuming that the mass loss detected during the 603 K decomposition peak corresponded exclusively to decomposition of the malachite phase. Sample B-2 was considered to contain pure aurichalcite. Results are given in Table 2, where the experimental mass losses are compared with those calculated from the proposed phase composition. A reasonable agreement was obtained between the experimental and predicted mass losses.

IR spectroscopy results

To gain more insight into the thermal decomposition of the precursor precipitates, sample T-2, which contains exclusively hydrotalcite, was treated at increasing temperature and characterized by XRD and IR techniques. Figure 5 shows the IR spectra obtained in the carbonate region (1800–400 cm^{-1}) after successive calcination of the sample for 2 h at various temperatures. The spectrum at 373 K exhibits three absorption bands, at 1530, 1400 and 840 cm^{-1}. The bands at 1530 and 1400 cm^{-1} have been attributed to CO_3^{2-} in the interlayer space in C_{3v} (pyramidal) or C_{3v} symmetry [18, 19]. The band at 840 cm^{-1} is assigned to the symmetric stretching of CO_2 [20]. Major structural changes were detected in the region 473–773 K. Above 473 K, the CO_3^{2-} was removed from hydrotalcite, as shown by the decrease in intensity of the bands at 1530 and 1400 cm^{-1}. At 773 K, the band at 840 cm^{-1} disappeared, while a new band developed at 500 cm^{-1}, attributable to the formation of CuO [21]. After calcination at 873 K, the IR spectrum did not reveal the presence of any CO_3^{2-} in the sample, and the peak at 500 cm^{-1}, corresponding to CuO, appeared more clearly defined. In brief, characterization of the decomposition of sample T-2 by IR spectroscopy confirmed the DTG/DTA/EGA results presented above: a proportion of the CO_3^{2-} is eliminated in the middle-temperature range, whereas the final decarbonation of the sample at temperatures above 773 K leads to the formation of mixed oxide products.

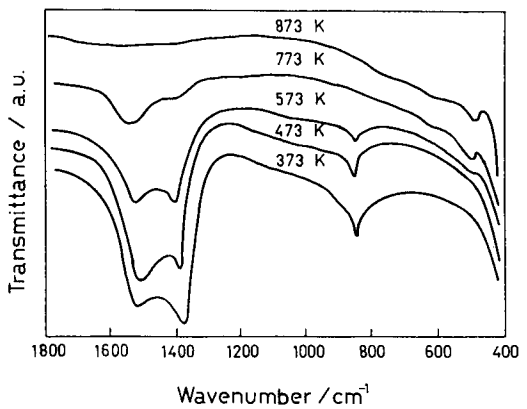

Fig. 5 IR spectra of sample T-2 heated at increasing temperatures

Decomposed precursors

After decomposition for 8 h at 873 K, the samples were characterized by XRD. Qualitatively, the phase composition of the mixed oxides did not depend significantly on the chemical compositions of the precursors. In fact, all the ternary samples and binary sample B-2 contained CuO and ZnO; an additional

$ZnAl_2O_4$ spinel-like phase was detected in samples T-1, T-2 and T-3. The diffractogram of binary sample B-1 exhibited a single crystalline phase of CuO.

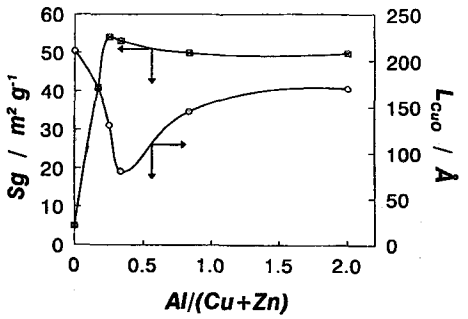

Fig. 6 Effect of the Al/(Cu+Zn) ratio on the CuO crystallite size (L_{CuO}) and the surface area (S_g) of the mixed oxides. All the samples contain 34 wt% of Cu

In contrast, the CuO crystallite size was greatly influenced by the chemical compositions of the precursors. Figure 6 presents the evolution of L_{CuO} as a function of atomic ratio Z=Al/(Cu+Zn). The lowest L_{CuO} value was obtained for sample T-2 (Z=0.33), which contains pure hydrotalcite. From an inspection of column 5 in Table 2, it is inferred that the mean crystallite sizes of CuO represented in Fig. 6 were related to the amount of hydrotalcite in the sample: the higher the hydrotalcite content, the lower the L_{CuO} value. The presence of hydrotalcite therefore appears necessary for the stabilization of CuO in a finely dispersed phase. This conclusion is in line with the results reported by Gherardi *et al.* [9] for similar catalysts used in the low-temperature synthesis of methanol. These latter authors attributed the influence of the hydrotalcite-like structure on the formation of very small CuO crystallites to the perfect distribution of the elements obtained inside the ternary structure. There is general agreement that hydrotalcite and related compounds do not reveal any segregation into regions of different composition [11].

Finally, the surface areas of the decomposed precursors as a function of Z are shown in Fig. 6. The S_g value increased markedly from 5 $m^2 g^{-1}$ (sample B-1, Z=0) to 53 $m^2 g^{-1}$ (sample T-2, Z=0.33), but subsequently did not change significantly for higher Z values. This can be explained by considering that the amount of amorphous Al_2O_3 phase increases with increasing Z, thereby compensating the simultaneous lowering of the surface area due to the formation of larger crystallites of CuO and ZnO.

Conclusions

The main conclusions of this study regarding the preparation and thermal decomposition of Cu–Zn–Al precursors in order to obtain water-gas shift catalysts can be summarized as follows:

i. The phase composition of Cu–Zn–Al hydroxycarbonate precursors containing 34 wt% of Cu depends greatly on the Al/Zn ratio. Homogeneous crystalline precursors appear only in a narrow range of Z=Al/(Cu+Zn).

ii. The thermal decompositions of the precursor precipitates occur mainly in three main endothermic transformations. In the first step, between 363 and 453 K, only the hydrotalcite-containing precursors decompose by eliminating the crystallization water of the hydrotalcite phase. Dehydration is achieved at low temperatures, below 453 K, causing disappearance of the hydrotalcite layered structure. In the range of the middle-temperature transformation (453–673 K), samples are progressively dehydroxylated up to total elimination of OH groups at 673 K. The loss of water is accompanied by removal of some of the CO_3^{2-} in two separate phenomena. In hydrotalcite-containing samples, dehydroxylation of adjacent OH groups in the same brucite layer starts at ca. 453 K, while the release of CO_3^{2-}, as CO_2, begins above 473 K. As a consequence, dehydroxylation overlaps with the onset of decarbonation. Finally, in the range 673–923 K, all the samples lose the strongly bonded CO_3^{2-} and are completely decarbonated, leading to the formation of the final mixed oxides.

iii. The mean crystallite size of the CuO in the resulting mixed oxides depends on the amount of hydrotalcite in the precipitate precursor: the higher the hydrotalcite content, the lower the L_{CuO} values. Hydrotalcite appears to be a preferential precursor structure for obtaining the CuO phase finely dispersed in the ZnO/Al_2O_3 matrix.

* * *

Support of this work by the Consejo Nacional de Investigaciones Científicas y Técnicas (CONICET, Argentina) is gratefully acknowledged.

References

1 D. C. Grenoble, M. M. Estadt and D. F. Ollis, J. Catal., 67 (1981) 90.
2 J. Nakamura, J. M. Campbell and C. T. Campbell, J. Chem. Soc. Faraday Trans., 86 (1990) 2725.
3 L. Lloyd, D. E. Ridler and M. V. Twigg, in M. V. Twigg (Ed.), Catalyst Handbook, 2nd Edition, Wolfe, London 1989, p. 283.
4 A. J. Marchi, J. I. Di Cosimo and C. R. Apesteguía, Proc. 4th Int. Symp. on Scientific Bases for the Preparation of Catalysts, Louvain-la-Neuve, Belgium, Pap. H-7, 1986.
5 J. I. Di Cosimo, A. J. Marchi and C. R. Apesteguía, J. Catal., 134 (1992) 594.
6 R. A. Hadden, P. J. Lambert and C. Ranson, Appl. Catal. A, 122 (1995) L1.
7 J. E. Baker, R. Burch and N. Yuquin, Appl. Catal., 73 (1991) 135.
8 M. J. L. Ginés and C. R. Apesteguía, Appl. Catal., A, 131 (1995) 283.
9 P. Gherardi, O. Ruggeri, F. Trifiro, A. Vaccari, G. Del Piero, G. Manara and B. Notari, in G. Poncelet, P. Grange and P. A. Jacobs (Eds.), Preparation of Catalysts III, Elsevier, Amsterdam 1983, p. 723.
10 H. F. W. Taylor, Min. Mag., 39 (1973) 304.
11 S. Miyata, Clays and Clay Minerals, 23 (1975) 369.

12 W. T. Reichle, S. L. Kang and D. S. Everhardt, J. Catal., 101 (1986) 253.
13 A. J. Marchi, J. I. Di Cosimo and C. R. Apesteguía, in J. M. Phillips and M. Ternan (Eds.), Proc. 9th Int. Congress on Catalysis, Chemical Institute of Canada, Ottawa 1988, Vol. 2, p. 529.
14 F. Rey, V. Fornés and J. M. Rojo, J. Chem. Soc. Faraday Trans., 88 (1992) 2233.
15 T. Sato, K. Kato, T. Endo and M. Shimada, React. Solids, 2 (1986) 253.
16 E. B. M. Doesburg, R. H. Hoppener, B. de Koning, X. Xiaoding and J. J. F. Scholten, in Preparation of Catalysts IV, B. Delmon, P. Grange, P. A. Jacobs and G. Poncelet Eds., Elsevier, Amsterdam 1987, p. 767.
17 D. S. Shishkov, N. A. Kassabova and K. N. Petkov, in Preparation of Catalysts III, G. Poncelet, P. Grange and P. A. Jacobs, Eds., Elsevier, Amsterdam 1983, p. 757.
18 J. Hernandez-Moreno, M. A. Ulibarri, J. L. Rendon and C. J. Serna, Phys. Chem. Mineral, 12 (1985) 34.
19 F. Cavani, F. Trifiro and A. Vaccari, Catal. Today, 11 (1991) 173.
20 T. Yamaoka, M. Abe and M. Tsuji, Mat. Res. Bull., 24 (1989) 1183.
21 N. Mc Devitt and W. Baum, Spectrochim. Acta, 20 (1963) 799.